

Reflected Shock Wave Bifurcation Detonation Initiation

Vahid Yousefi-Asli, Gaby Ciccarelli
Queen's University
Kingston, Ontario Canada

1 Introduction

Flame acceleration in an obstructed channel leading to deflagration-to-detonation transition (DDT) has been studied extensively over the years in connection with explosion safety. In this geometry, it is observed that a fast-flame, consisting of a precursor shock and turbulent flame, that travels at roughly one-half the CJ detonation velocity forms before the onset of detonation [1]. In the traditional setup of a round tube equipped with orifice plates, the onset of detonation normally occurs with shock reflection off the obstacle face [2]. The ensuing detonation propagation, characterized by a large the CJ detonation velocity deficit, is the result of repeating detonation failure and re-initiation. The key mechanism for detonation re-initiation in this mechanism is the reflection of the decoupled shock off the obstacle face [3]. In shock tube experiments detonation either occurred promptly, or was delayed following shock reflection [4]. Voevodsky et al. [5] described the delayed initiation at lower reflected shock temperatures as originating from the merging of multiple flame kernels producing a reaction front that accelerates leading to “mild” detonation initiation. Meyer and Oppenheim [6] showed that for strong ignition a detonation forms promptly and uniformly following shock reflection; whereas, mild ignition is characterized by multiple flame ignition kernels leading to DDT, as hypothesized in [5].

Merkel and Ciccarelli [7] recently reported weak detonation initiation data for methane-air from high-speed schlieren video obtained in a 7.6 cm square cross-section shock tube. It is very difficult to interpret schlieren video as it provides an integrated representation across the channel width; even when it is clear that detonation initiation occurs at a point, it is not possible to determine where in the cross-section it occurs. Many recent studies link detonation initiation with shock bifurcation that occurs when the reflected shock interacts with the post-incident shock boundary layer, the bifurcation produces the λ -shock structure shown in Fig. 1. A stagnation bubble forms when the boundary layer does not have sufficient energy to penetrate the reflected shock region. Since the flow through the two oblique shocks results in less momentum loss than through the main reflected shock, colder gas enters into the region of hot gas at the end wall that can affect the ignition time measured in experiments. There is no clear consensus between numerical and the very limited experimental studies on the role of reflected shock bifurcation on detonation initiation. The objective of this study is to investigate detonation initiation

driven by shock reflection using schlieren through the side wall and simultaneous self-luminous visualization through the end wall in order to identify the mechanism of detonation initiation.

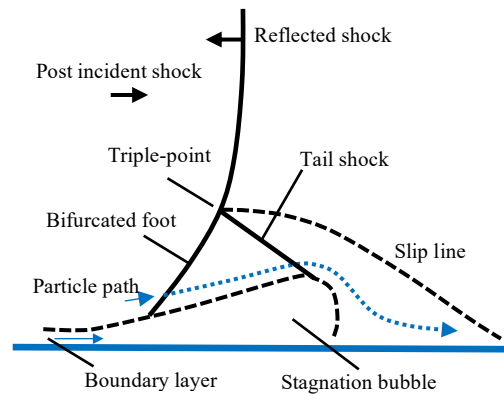


Figure 1: Schematic showing reflected shock bifurcation in a fixed reference frame. The blue dotted line shows a particle path through the bifurcated foot.

2 Experimental

Experiments were performed in a 5 m long shock tube with a 76.2 mm square-cross driven section, and a 2 m long, 100 mm inner-diameter driver section. There is a 0.72 m long square-to-circular transition section immediately after the diaphragm and an optically accessible test section at the end of the driven section. A double-diaphragm precisely controlled the burst pressure, where the diaphragms were cut from 1.6 mm thick, 1100 aluminum sheets. A symmetric four-petal opening was achieved by stamping the diaphragm with an X shaped indent. Testing was carried out primarily with nitrogen diluted stoichiometric ethylene-oxygen, e.g., $C_2H_4+3O_2+3N_2$. The incident shock Mach number was varied primarily by changing the nitrogen/hydrogen driver gas composition. An 83% nitrogen and 17% argon buffer gas was required to separate the hydrogen containing driver gas from the oxygen containing test gas. This composition was selected to give the same molecular weight as the test gas; the matching density prevented a gravity current from forming when the buffer gas was introduced into the driven section. The test mixture was prepared by the method of partial pressures in a stainless steel mixing tank equipped with a stirring propeller driven by a Parr magnetic driver that was powered by an electric motor.

The novel optical test section permits simultaneous visualization from two perspectives. Windows on the front and back side-walls were used for traditional high-speed schlieren, and a window at the end wall for synchronized end-view self-luminous video. A Photron SA5 operated at 100,000 fps was used for the schlieren side-view and a Photron SAX, operated at twice the frame rate of the SA5, was used for the end-view visualization. To avoid replacing the windows after each test due to the high reflected shock pressure and temperature, the windows were covered with sacrificial 2.4 mm thick polycarbonate windows that were replaced after each test. The test section was equipped with three flush-mounted PCB Piezotronics 114B26 pressure transducers located on the top wall 20 mm, 96.2 mm and 172.4 mm from the end wall. For select tests, a soot-coated 0.5 mm thick aluminum foil was taped to the top and bottom walls of the shock tube

3 Results and Discussion

Figure 2 presents the measured ignition delay time (IDT) as a function of the inverse reflected equilibrium temperature for nitrogen-diluted stoichiometric ethylene-oxygen. The reflected shock temperature was calculated from the measured incident shock velocity, calculated based on the time-of-

arrival at the last two pressure transducer. All the weak mode IDT data provided in Fig. 2 is from schlieren video that provides the time for flame ignition (FI - open circles) and detonation initiation (DI - closed circles). For the strong mode, the IDT data is based on video and pressure recording (reflecting wall was moved to the last PT for these tests). The error bars for the video data represent the 10 μ s time between frames, for the pressure transducer the uncertainty is 1 μ s, i.e., the rise-time of the transducer. Also provided in Fig. 2 for reference is the induction time calculated using the Caltech Shock and Detonation Toolbox constant pressure (CP) model and the San Diego chemical kinetic mechanism [8]. The reflected pressure for all the data lies in the range 6-8 bar. For the strong initiation mode, there is good agreement between the measurement and CP model; however, for the weak mode the experimentally measured detonation initiation time is significantly shorter than the model prediction. As discussed next, this is due to multi-dimensional effects that are not taken into account in the model. A systemic study showed there was no measurable difference in the IDT when a soot foil was or was not present.

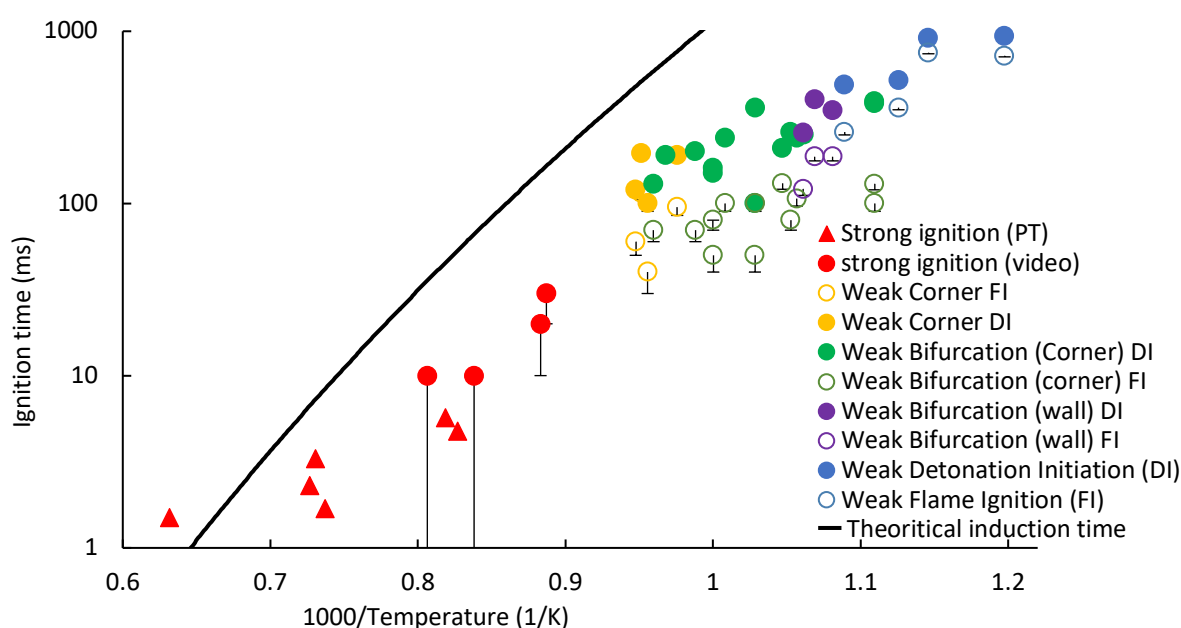


Figure 2: Experimental video-based flame ignition (open circles) and detonation initiation (closed circles) delay times measured from the time of shock reflection in $C_2H_4+3O_2+3N_2$. Strong ($1000/T < 0.9 \text{ K}^{-1}$) and weak detonation ($1000/T > 0.95 \text{ K}^{-1}$) initiation modes. Red horizontal line marker corresponds to the IDT based on the rapid rise in the pressure signal. The line represents the CP reaction-model induction times obtained using the San Diego chemical kinetics mechanism [8].

A novel weak initiation mode associated with reflected shock bifurcation was identified using the stereo visualization images, see Fig. 3. There are soot foils on the top and bottom walls. The slightly curved reflected shock and the bifurcated foot (see the schematic in Fig. 1) propagating along the front and back windows generate a thick dark band moving to the right. In addition, immediately to the left of the band is the density disturbance associated with the shock bifurcation stagnation-bubble on the front and back windows reported in [9]. Following shock reflection, a flame forms at the end wall, outlined by a dotted line in schlieren image 1. There is no light emission from the flame captured in the end view, except for the incandescence from the soot lofted from the bottom wall inside the flame. In the schlieren image 2, a flame front (highlighted by an arrow) emerges that propagates along the bottom wall boundary layer. The end view images clearly show that this flame runs along the left-bottom corner of the shock tube (back window), for this reason the flame is slightly obscured by the soot from the bottom wall lofted behind the incident shock. A second bright spot appears in the end view image 4, close to the bottom-right corner, that is of no consequence to DDT. The flame in the bottom-left corner propagates from the

end wall reaching the bifurcation stagnation bubble in schlieren image 4. The flame spreads quickly through the stagnation bubble to form a flame ball. The flame ball rapidly expands, where the velocity of the top segment of the flame between images 5 and 6 is 850 m/s. This velocity is supersonic relative to the post-reflected shock condition. Detonation initiation occurs between images 6 and 7, the smooth outline of the detonation can be seen in the schlieren and end view image 7. From the schlieren images, the velocity of the segment of the detonation wave propagating in the vertical direction is estimated to be 2180 m/s.

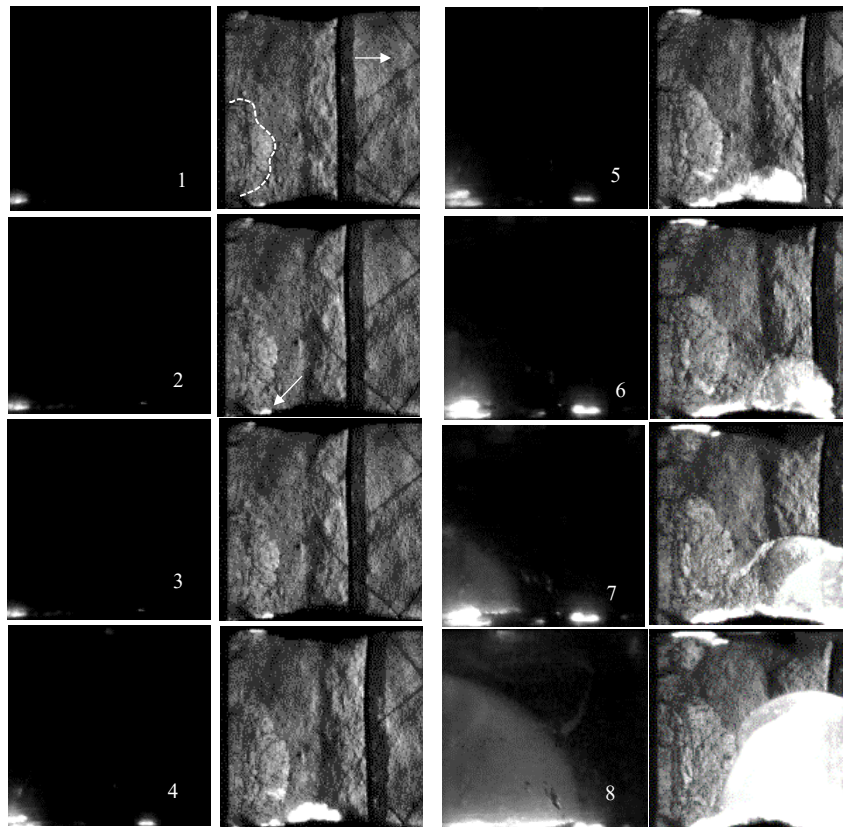


Figure 3: Stereo imaging of weak-bifurcation initiation mode for reflected shock conditions 958 K and 6.6 bar. Left: self-luminous end view, right: schlieren side view (test 160, 10 μ s between images).

The soot foil positioned on the upper wall and the schlieren image captured just after the onset of detonation are provided in Fig. 4 (from a different test than the one in Fig. 3). The bifurcated reflected shock and multiple flames near the end wall are visible in the schlieren image. The lofted soot accumulates inside the stagnation bubble along the top and bottom walls blocking the schlieren light, making the bubble visible as a shadow in the image. The location of the stagnation bubble along the front and back walls can also be identified by the schlieren light disturbance before and after the reflected shock. In Fig. 4, the soot particle-filled stagnation bubble along the top wall appears in front of the detonation bubble, indicating that the detonation propagates transversely along the top wall from the back to the front window. The orientation of the patches of detonation cells highlighted in Fig. 4 is consistent with this initiation location. The detonation bubble is centered with the stagnation bubble, similar to that observed in Fig. 3; therefore, detonation initiation most likely followed the rapid combustion through the stagnation bubble.

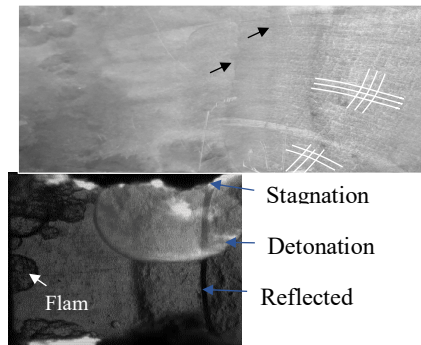


Figure 4: Upper wall soot foil (top) and schlieren image (bottom) of weak-bifurcation initiation mode for a reflected shock temperature of 955K (test 118).

Horizontal streaks in the soot appear in the region between two dark lines on the foil (see arrow tips). Based on the corresponding position of the stagnation bubble and the left line, it appears that the line is generated by the detonation wave traversing the leading edge of the stagnation bubble on the upper wall. The right-line corresponds to the start of the detonation cell structure, i.e., cells only appear to the right of the line. Interestingly, no cells appear to the left of this line despite the fact that the detonation propagates through the region. This means that the reflected shock wave, or more specifically the stagnation bubble, lifts the remaining soot off the foil so no cell imprint is created by the passage of the detonation wave. Note, the two lines in question lean forward slightly because as the detonation propagates across the channel (back to front) the stagnation bubble moves forward with the reflected shock.

At a higher reflected shock temperature, flame ignition typically occurs in one of the end wall corners, as is the case for the test in Fig. 4. For lower reflected shock temperatures, flame ignition occurs away from the end wall in the boundary layer along one of the tube edges. This is the case for the test results shown in Fig. 5, where flame ignition occurs on the top wall in image 2 and slightly further along on the bottom wall in image 3, see arrows in both images. Based on similar results (end wall video was not recorded for this test) flame ignition occurs and propagates axially along a corner. Once the flame front enters the stagnation bubble it rapidly accelerates due to the circulation and high level of vorticity. A detonation wave initiates between images 8 and 9, and it quickly reaches the bottom stagnation bubble gas before it has a chance to produce a detonation.

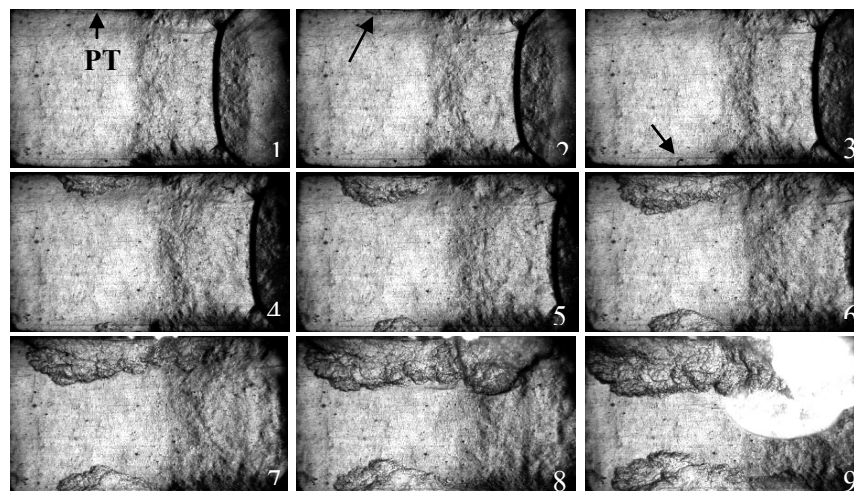


Figure 5: Schlieren side view of weak-bifurcation initiation mode starting on the side wall for reflected shock conditions 925 K and 7.1 bar. The white line corresponds to the location on the top wall nearest to the end wall (test 112, 13.33 μ s between images)

Provided in Fig. 6 is the pressure-time history recorded from the test shown in Fig. 5. The location of the pressure transducer at 20 mm is shown in image 1. The pressure transducer at 96.2 mm is near the right-edge of the field-of-view in Fig. 5. The rapid pressure-rise associated with the passage of the incident shock is observed sequentially in the blue, red and then black trace, and the pressure-rise associated with the reflected shock is observed in the reverse sequence. The second pressure-rise occurring in the black trace (indicated by an “A” in Fig. 6) corresponds to the reflected shock bifurcation foot. A pressure rise follows reaching a peak (denoted by B) as the stagnation bubble passes over the pressure transducer. The peak at B corresponds to the end of the stagnation bubble where the flow direction is towards the transducer face. After the stagnation bubble passes, the pressure remains constant for about 0.2 ms at the theoretical reflected shock pressure, and is followed by a very abrupt, large magnitude pressure-rise associated with the detonation. When the reflected shock passes over the second pressure transducer (red pressure trace) the slope of the pressure-rise is reduced. This is because as the reflected shock propagates, the length of the stagnation bubble lengthens (so does the triple point height and the distance between the oblique shocks). The large magnitude detonation pressure-rise occurs before the peak-pressure produced by the stagnation bubble is achieved. This indicates that the detonation initiation occurs very close to the second pressure transducer. The first pressure transducer experiences a pressure increase (see C) before the arrival of the detonation wave, which could be related to the flame propagation along the corner observed in Fig. 5 leading up to detonation initiation.

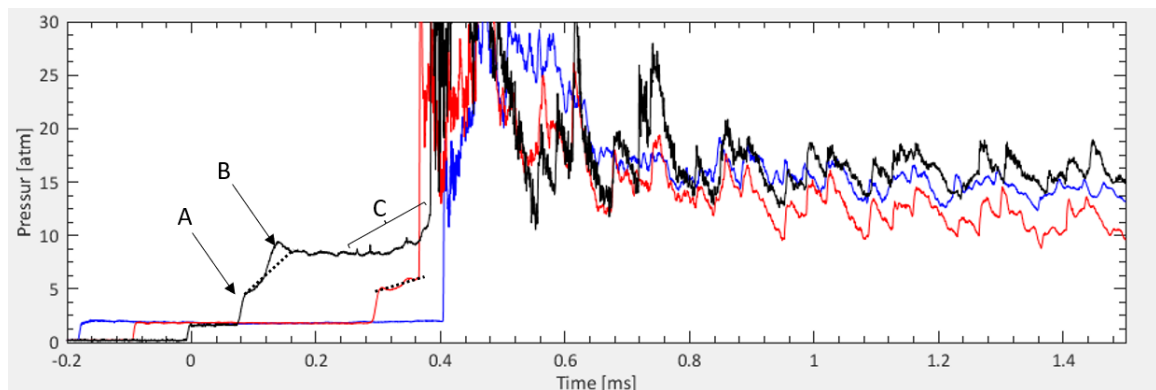


Figure 6: Pressure traces corresponding to the schlieren in images in Fig. 5. Pressure transducers are located 20 mm (black line), 86 mm, (red line), and 172.4 mm (blue line) from the end wall.

4 Conclusions

Using the novel visualization technique, the study revealed a new weak initiation mechanism that involved the propagation of a flame along one, or more, corners that reach and quickly spread through the stagnation bubble after the bifurcation foot. The rapid burning and expansion of the bubble gas results in transition to detonation. The video images show the detonation emerging symmetrically from the stagnation bubble. The rapid flame propagation along the corner and flame spread in the stagnation bubble are currently under investigation using 3D numerical simulations.

References

- [1] Peraldi O, Knystautas R, Lee, JH. (1988) Criterion for transition to detonation in tubes, Symp. Combust. Proc. 21: 1629-1637.
- [2] Rainsford G, Singh Aulakh DJ, Ciccarelli G. (2018) Visualization of detonation propagation in a round tube equipped with repeating orifice plates, Combust. Flame, 198: 205-221.
- [3] Kellenberger M, Ciccarelli G. (2018) Advancements on the propagation mechanism of a detonation wave in an obstructed channel, Combust. Flame, 191: 195–209.

- [4] Strehlow RA, Cohen A. (1962) Initiation of detonation, Phys. Fluids, 5: 97-101.
- [5] Voevodsky V, Soloukhin R. (1965) On the mechanism and explosion limits of hydrogen-oxygen chain self-ignition in shock waves, Symp. Combust. Proc. 10: 279-283.
- [6] Meyer J, Oppenheim A. (1971) On the shock-induced ignition of explosive gases, Symp. Combust. Proc. 13: 1153-116.
- [7] Merkel C, Ciccarelli G. (2020) Visualization of methane-air ignition behind a reflected shock wave, Fuel, 271: 117617.
- [8] Chemical-Kinetic Mechanisms for Combustion Applications, UC at San Diego (<http://combustion.ucsd.edu>).
- [9] Mark H. The interaction of a reflected shock wave with the boundary layer in a shock tube, NACA TM 1418, 1958.